Наносистеми, наноматеріали, нанотехнології
Nanosistemi, Nanomateriali, Nanotehnologii
2025, т. 23, № 2, сс. 449–465
https://doi.org/10.15407/nnn.23.02.0449

PACS numbers: 61.46.Bc, 68.43.Bc, 71.15.Mb, 73.20.Hb, 73.22.Lp, 81.07.Nb, 85.30.De

Smart Nanocomposites of ZnO & ZnS as Potent Semiconductors Through Hydrogen-Bonded Engineering in Transistors

Fatemeh Mollaamin

Department of Biomedical Engineering,
Faculty of Engineering and Architecture,
Kastamonu University,
Kastamonu, Turkey

We employ first-principles calculations to investigate the structural stability and electronic properties of cubic zinc oxide (ZnO) and zinc sulphide (ZnS) heteroclusters adsorbed with H_2O molecule. A comprehensive investigation on H_2O grabbing by ZnO/ZnS heteroclusters is carried out using DFT computations at the CAM–B3LYP–D3/6–311+G(d, p) level of theory. The notable fragile signal intensity close to the parallel edge of the nanocluster sample might be owing to H/OH-binding-induced non-spherical distribution of ZnO or ZnS heterocluster. The hypothesis of the energy absorption phenomenon is confirmed by density distributions of CDD, TDOS/PDOS/OPDOS, and LOL for ZnO/ZnO–H_2O or ZnS/ZnS–H_2O. A vaster jointed area is engaged by an isosurface map for H/OH adsorption on ZnO or ZnS surface towards formation of ZnO–H_2O or ZnS–H_2O complex due to labelling atoms of O1, Zn15, O27 or S27, H29, H30. Therefore, it can be considered that zinc in the functionalized ZnO or ZnS might have more impressive sensitivity for accepting the electrons in the process of H/OH adsorption. It is considerable that, when all surface atoms of ZnO or ZnS are coated by OH and H groups, the semiconducting behaviour is recovered. Our results open up the possibility of tailoring the electronic properties by controlling the surface adsorption sites.

Ми використовуємо розрахунки з перших принципів для дослідження структурної стабільности й електронних властивостей кубічних гетерокластерів оксиду Цинку (ZnO) та сульфіду Цинку (ZnS), адсорбованих із молекулою H_2O. Комплексне дослідження захоплення H_2O гетерокластерами ZnO/ZnS було проведено з використанням DFT-обчислень на теоретичному рівні CAM–B3LYP–D3/6–311+G(d, p). Примітна слабка інтенсивність сиґналу поблизу паралельного краю зразка нанокластера може бути пов'язана з несферичним розподілом гетерокластера ZnO або ZnS, індукованим зв'язуванням H/OH. Ґіпотезу про явище абсорбції енергії було підтверджено розподілами густини CDD, TDOS/PDOS/OPDOS і LOL для

ZnO/ZnO–H_2O або ZnS/ZnS–H_2O. Ширша з'єднана область охоплюється ізоповерхневою мапою для адсорбції H/OH на поверхні ZnO або ZnS задля утворення комплексу ZnO–H_2O або ZnS–H_2O завдяки маркувальним атомам O1, Zn15, O27 або S27, H29, H30. Отже, можна вважати, що Цинк у функціоналізованому ZnO або ZnS може мати вражаючу чутливість щодо прийняття електронів у процесі адсорбції H/OH. Важливо, що, коли всі поверхневі атоми з ZnO або ZnS покриті групами OH і H, напівпровідникова поведінка відновлюється. Наші результати відкривають можливість налаштування електронних властивостей шляхом контролю вузлів поверхневої адсорбції.

Key words: cubic ZnO/ZnS heteroclusters, semiconductor, H/OH adsorption, first-principles calculations.

Ключові слова: кубічні гетерокластери ZnO/ZnS, напівпровідник, адсорбція H/OH, першопринципні розрахунки.

(Received 6 December, 2024)

1. INTRODUCTION

Zinc oxide (ZnO) is a promising semiconductor material for various applications ranging from optoelectronics to biomedicine, attributed to its wide direct band gap, high excitons-binding energy, high mobility, and high quantum efficiency. To improve further the performance of ZnO devices, plasma treatment is a common method for surface modification [1–4]. The luminescence properties of ZnO after plasma treatment are significantly changed, including ultraviolet (UV) luminescence, visible luminescence, and recombination mechanism [5–11].

Optical properties are improved significantly by H plasma, with negligible alteration in thickness. Although no chemical reaction is introduced, emission intensity is enhanced by Ar plasma by eliminating the non-radiative recombination centres. Furthermore, H and Ar plasma also induce strong exciton localization, leading to significant broadening of the UV spectrum [12–15].

However, replicating or applying the reported improvement in plasma treatments for ZnO often proves challenging. This difficulty arises from several factors, including the diverse properties of ZnO samples, which encompass thin films, single crystals and nanostructures grown through various methods. Moreover, the specific effects of plasma treatments using different gases remain unclear, as each type of gas plasma exhibits unique interactions. Consequently, it is crucial to conduct a systematic comparison of the influence of various plasma gases on the optical and electrical properties and to identify accurately the specific defects affected [16–21].

Transparent and superhydrophilic materials are indispensable for their self-cleaning function, which has become an increasingly popular research topic, particularly in photovoltaic (PV) applications. It was reported hydrophilic and superhydrophilic ZnO by varying the morphology for use as a self-cleaning coating for PV applications [22].

The researchers have applied molecular dynamics simulations through a reactive force field for ZnO–H_2O ambient. The force-field parameters were fitted to a dataset of energies, geometries and charges derived from density functional theory calculations. The applied model has provided a good fit to the quantum mechanics reference data for the ZnO–H_2O system that was present in the dataset. The force field has been used to study how H_2O is adsorbed, molecularly or dissociatively, at monolayer coverage on flat and stepped ZnO surfaces, at different temperatures. The results show that structures that promote hydrogen bonding are favoured and that the presence of steps promotes an increased level of hydroxylation in the water monolayers [23].

The cubic form of zinc sulphide (ZnS) is the prototype II–VI semiconductor with smallest lattice constant of $a_0 = 5.4102$ Å at 300 K and the primarily candidate for UV-light emitting devices because of its large band-gap energy around $\cong 3.7$ eV at room temperature [24].

Many research groups have attempted to dope anions and cations into the ZnO or ZnS lattice, which helps to reach various complex applications since its electronic structure and characteristics may be significantly adjusted. The enhanced catalytic properties reveal the synergy between ZnO and ZnS functional nanomaterials, which upgrade the electron–hole pair, resulting in an enhanced catalytic performance under the visible region. Notably, the ZnO-based ZnS nanocomposite was prepared by a wet chemical method without any template. The template method is not sensitive to the preparation conditions, is easy to operate and implement, and controls nanomaterials' structure, morphology, and particle size through the template material. Generally, the outstanding photocatalytic performance of wurtzite ZnO and ZnS semiconductor and their composite under visible light irradiation could be attributed to synergistic effects, when coupled with other metal oxide semiconductor. The present study is a part of our ongoing research to understand the solar energy conversion/harvesting directions. We reported a facile synthesis of ZnS and ZnO nanoparticles and their nanocomposites by the wet chemical method [25–29].

In this work, we analysed the effect of H_2O adsorption on the properties of ZnO or ZnS heterocluster via the density of state, charge distribution, bond orders and HOMO–LUMO orbitals using DFT studies. The optimized ZnO or ZnS is shown in Fig. 1, *a*, *b*,

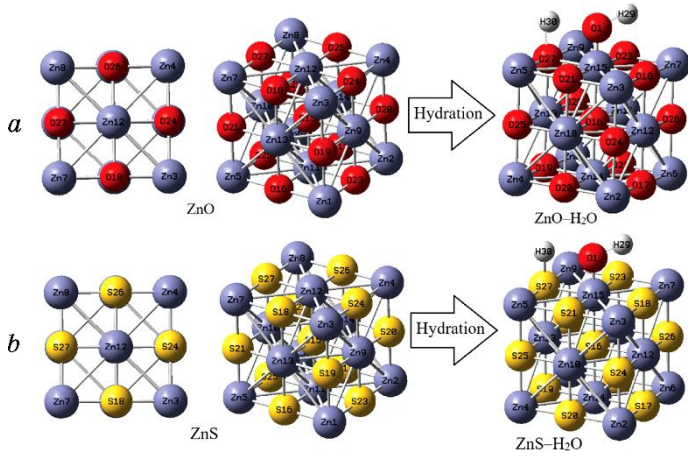

Fig. 1. Characterization of (*a*) ZnO/ZnO–H_2O and (*b*) ZnS/ZnS–H_2O heteroclusters through a labelled ring in clockwise manner including H, O, S, Zn towards H_2O adsorption.

and the Zn and O or S atoms are also numbered to characterize the reaction pathway.

2. THEORY, MATERIALS AND COMPUTATION

The hydration of ZnO or ZnS and formation of ZnO–H_2O or ZnS–H_2O heterocluster was calculated within the framework of first-principles calculation based on density functional theory (DFT) (Fig. 1). The rigid potential energy surface using density functional theory [30–43] was performed due to Gaussian 16 revision C.01 program package [44] and GaussView 6.1 [45]. The coordination input for energy storage on the solar cells has applied 6–311+G(*d*, *p*) and EPR–3 basis sets.

First, we optimized the structural parameters of the nanocluster of ZnO or ZnS and hydrated nanocluster of ZnO–H_2O or ZnS–H_2O for obtaining the highest short-circuit current density. Figure 1 shows the process of H_2O adsorption on nanocluster of ZnO or ZnS which is varied to maximize the absorption in the active region. This is a utility used to calculate ring area and perimeter, since ring area is sometimes involved in wave-function analysis. In this function, it is needed to input the index of the atoms in the ring in clockwise manner, which can conclude the total ring area and total ring perimeter for a tailored ring as 9.4242 Å and 12.2796 $Å^2$ for ZnO (Fig. 1, *a*) and 9.4240 Å and 12.2794 $Å^2$ for ZnS, respectively (Fig. 1, *b*).

3. RESULTS AND DISCUSSION

In this article, the data has evaluated the efficiency of ZnO or ZnS in H_2O medium through energies, geometries and charges derived from density functional theory calculations. The applied model has provided a good fit to the quantum mechanics reference data for the ZnO–H_2O or ZnS–H_2O systems that was present in the dataset. The force field has been used to study how water is adsorbed molecularly at monolayer coverage on ZnO or ZnS surfaces.

The amounts of charge-density differences 'CDD' is measured by considering isolated atoms or noninteracting ones. The mentioned approximation can be the lightest to use because the superposition value may be received from the primary status of the self-consistency cycle in the code that carries out the density functional theory (Fig. 2, *a*, *a*′, *b*, *b*′) [46]. Figure 2, *a*, *b* indicates all Zn, O or S atoms of ZnO or ZnS fluctuating around –9 to –1 Bohr. In Figure

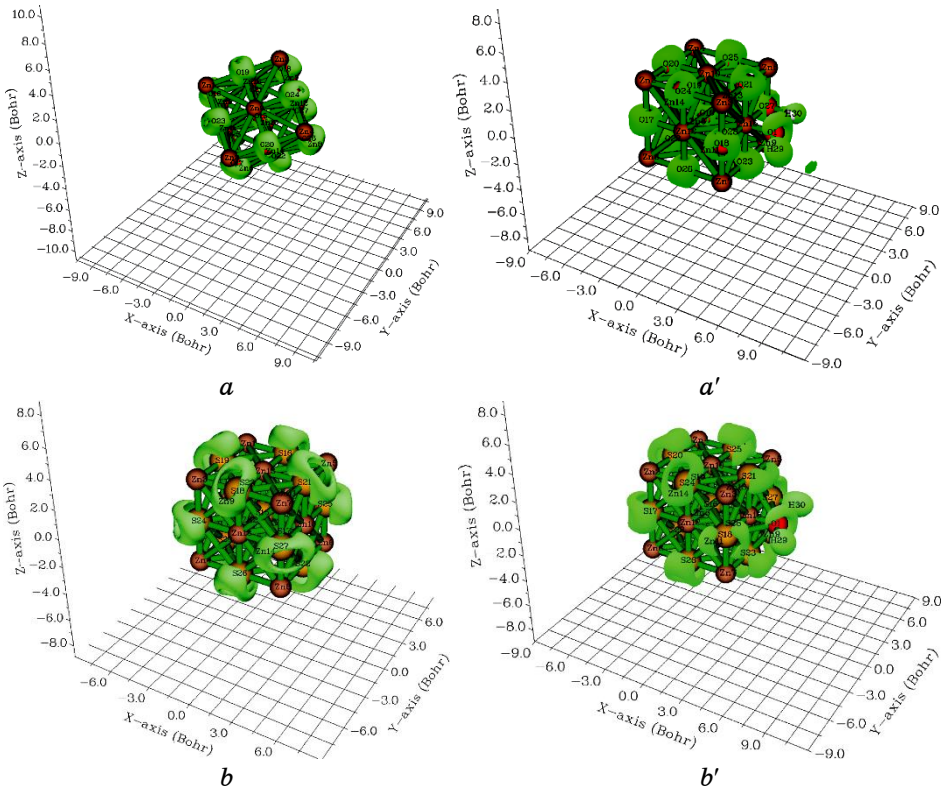

Fig. 2. CDD graphs for heteroclusters of (*a*) ZnO, (*a*′) ZnO–H_2O, (*b*) ZnS, and (*b*′) ZnS–H_2O.

2, a', b', the atom of Zn15, O27 or S27 from ZnO–H_2O or ZnS–H_2O and O1, H29, H30 from H_2O molecule accompanying other Zn, O or S atoms from ZnO–H_2O or ZnS–H_2O have shown the fluctuation around –1 to +1 Bohr and –9 to +1 Bohr, respectively.

Furthermore, atomic charge during H_2O adsorption by ZnO or

TABLE 1. The atomic charge (Q/coulomb) for heteroclusters of ZnO and ZnS through H/OH adsorption and formation of ZnO–H_2O and ZnS–H_2O heteroclusters.

ZnO		ZnO–H_2O		ZnS		ZnS–H_2O	
Atom	Charge	Atom	Charge	Atom	Charge	Atom	Charge
Zn1	0.7141	O1	–0.5958	Zn1	–0.5916	O1	–0.6526
Zn2	0.7139	Zn2	0.6972	Zn2	–0.5915	Zn2	–0.5742
Zn3	0.7135	Zn3	0.7278	Zn3	–0.5915	Zn3	–0.5431
Zn4	0.7141	Zn4	0.7273	Zn4	–0.5914	Zn4	–0.5535
Zn5	0.7141	Zn5	0.5927	Zn5	–0.5914	Zn5	–0.4722
Zn6	0.7135	Zn6	0.6958	Zn6	–0.5913	Zn6	–0.5761
Zn7	0.7140	Zn7	0.7113	Zn7	–0.5913	Zn7	–0.5656
Zn8	0.7140	Zn8	0.7264	Zn8	–0.5912	Zn8	–0.5528
Zn9	1.7451	Zn9	0.5981	Zn9	–0.4176	Zn9	–0.4722
Zn10	1.7450	Zn10	1.7256	Zn10	–0.4179	Zn10	–0.4578
Zn11	1.7471	Zn11	1.7376	Zn11	–0.4175	Zn11	–0.4581
Zn12	1.7471	Zn12	1.8835	Zn12	–0.4176	Zn12	–0.4646
Zn13	1.7461	Zn13	1.9004	Zn13	–0.4175	Zn13	–0.5131
Zn14	1.7460	Zn14	1.6986	Zn14	–0.4176	Zn14	–0.3470
O15	–1.5357	Zn15	1.4867	S15	0.6704	Zn15	–2.6670
O16	–1.2210	O16	–1.5460	S16	0.5475	S16	0.7342
O17	–1.2210	O17	–1.2236	S17	0.5473	S17	0.6123
O18	–1.2210	O18	–1.2143	S18	0.5473	S18	0.7932
O19	–1.2209	O19	–1.2232	S19	0.5475	S19	0.8517
O20	–1.2209	O20	–1.2259	S20	0.5473	S20	0.5726
O21	–1.2209	O21	–1.1381	S21	0.5471	S21	1.1263
O22	–1.2209	O22	–1.2260	S22	0.5469	S22	0.5741
O23	–1.2210	O23	–1.1370	S23	0.5475	S23	1.1166
O24	–1.2210	O24	–1.2155	S24	0.5473	S24	0.5695
O25	–1.2210	O25	–1.2183	S25	0.5471	S25	0.6185
O26	–1.2210	O26	–1.2157	S26	0.5471	S26	0.5693
O27	–1.2210	O27	–1.1850	S27	0.5469	S27	0.2986
		O28	–1.2183			S28	0.6184
		H29	0.2973			H29	0.4588
		H30	0.3764			H30	0.3556

ZnS towards formation of $ZnO–H_2O$ or $ZnS–H_2O$ (Table 1) was discussed. The atomic charge of Zn, O or S, and H/OH adsorbed on ZnO or ZnS have been measured. The values detect that, with adding H_2O, the negative atomic charges of oxygen atoms of O16, O17, O18, O19, O20, O21, O22, O23, O24, O25, O26, O27, O28 in $ZnO–H_2O$ have changed through coating of ZnO with H/OH. In fact, $ZnO–H_2O$ has shown more efficiency than ZnO for admitting the electron from electron donor of O16 to O28 (Table 1 and Fig. 3, *a*).

However, the negative atomic charge of zinc atoms and loss of

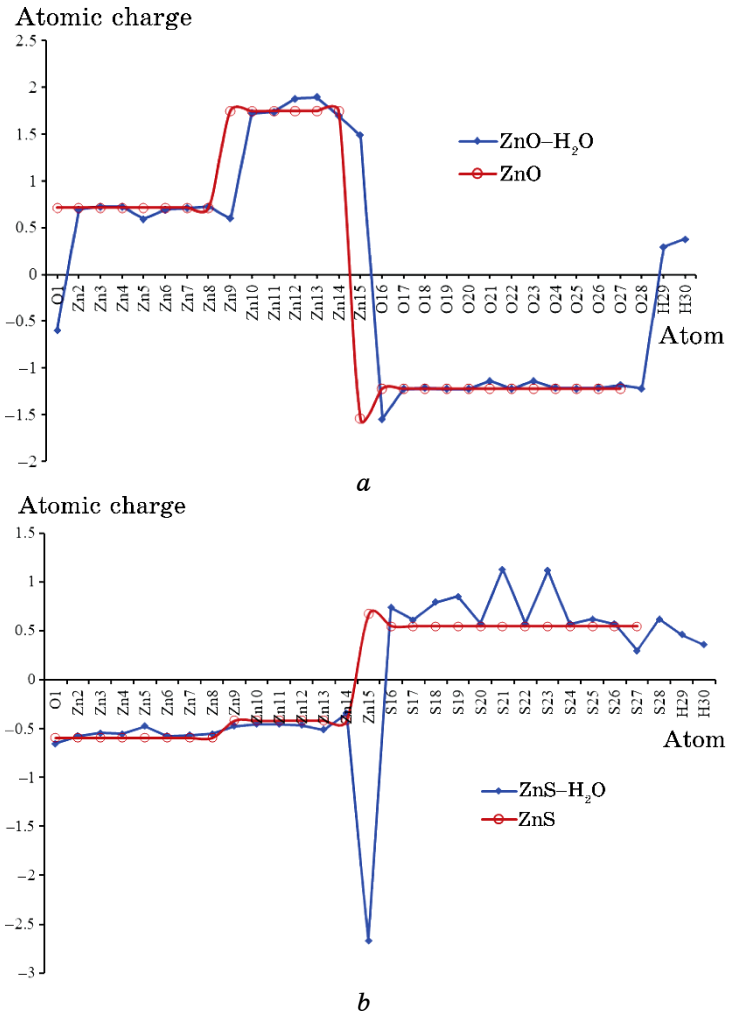

Fig. 3. The fluctuation of atomic charge (*Q*/coulomb) for (*a*) ZnO/$ZnO–H_2O$ and (*b*) ZnS/$ZnS–H_2O$.

negative atomic charge of sulphur in ZnS/ZnS–H_2O have been observed through Table 1 and Fig. 3, *b*. The changes of charge density analysis in the adsorption process have illustrated that ZnO and ZnO–H_2O nanoclusters have shown the 'Bader charge' of –1.747 and –1.900 coulomb, respectively. The differences of charge density for these structures are measured as $\Delta Q_{\text{ads.ZnO–H}_2\text{O}} = -0.153$ coulomb. The changes of charge density analysis in the adsorption process have illustrated that ZnS and ZnS–H_2O nanoclusters have shown the 'Bader charge' of –0.670 and –2.667 coulomb, respectively. The differences of charge density for these structures are measured as $\Delta Q_{\text{ads.ZnS–H}_2\text{O}} = -1.997$coulomb.

To understand better the different adsorption characteristics of ZnO/ZnO–H_2O and ZnS/ZnS–H_2O heteroclusters, total density of states (TDOS) using the Multiwfn program [45] has been measured. This parameter can indicate the existence of important chemical interactions often on the convex side (Fig. 4, *a*, *a*′, *b*, *b*′). In isolated system (such as molecule), the energy levels are discrete, the concept of density of state (DOS) is supposed completely valueless in this situation. Therefore, the original total DOS (TDOS) of isolated system can be written as follows [47]:

$$\text{TDOS}\ (E) = \sum_i \delta\left(E - \int_i\right), \tag{1}$$

$$G(x) = \frac{1}{c\sqrt{2\pi}} e^{-\frac{x^2}{2c^2}}, \text{ where } c = \frac{\text{FWHM}}{2\sqrt{2\ln x}}. \tag{2}$$

Moreover, the curve map of broadened partial DOS (PDOS) and overlap DOS (OPDOS) are valuable for visualizing orbital composition analysis, PDOS function of fragment *A* is defined as

$$\text{PDOS}_A(E) = \sum_i \Xi_{i,A} F\left(E - \int_i\right), \tag{3}$$

where $\Xi_{i,A}$ is the composition of fragment *A* in orbital *i*. The OPDOS between fragment *A* and *B* is defined as

$$\text{OPDOS}_{A,B}\ (E) = \sum_i X^i_{A,B} F\left(E - \in_i\right), \tag{4}$$

where $X^i_{A,B}$ is the composition of total cross term between fragment *A* and *B* in orbital *i*.

In the TDOS map, each discrete vertical line corresponds to a molecular orbital (MO), the dashed line highlights the position of HOMO. The curve is the TDOS simulated based on the distribution of MO energy levels. In the negative part, the region around –0.60 to –0.80 a.u. has obviously larger state density than other regions

for ZnO and ZnO–H_2O nanoclusters (Fig. 4, *a*, *a*′). However, it has been shown a larger state density through pointed peaks for ZnO–H_2O (Fig. 4, *a*′) than ZnO (Fig. 4, *a*) around –0.20 to –0.40 a.u.

It is remarkable that, when all surface atoms of ZnO are coated by OH and H groups, the semiconducting behaviour is recovered. Our results open up the possibility of tailoring the electronic properties by controlling the surface adsorption sites. In the positive

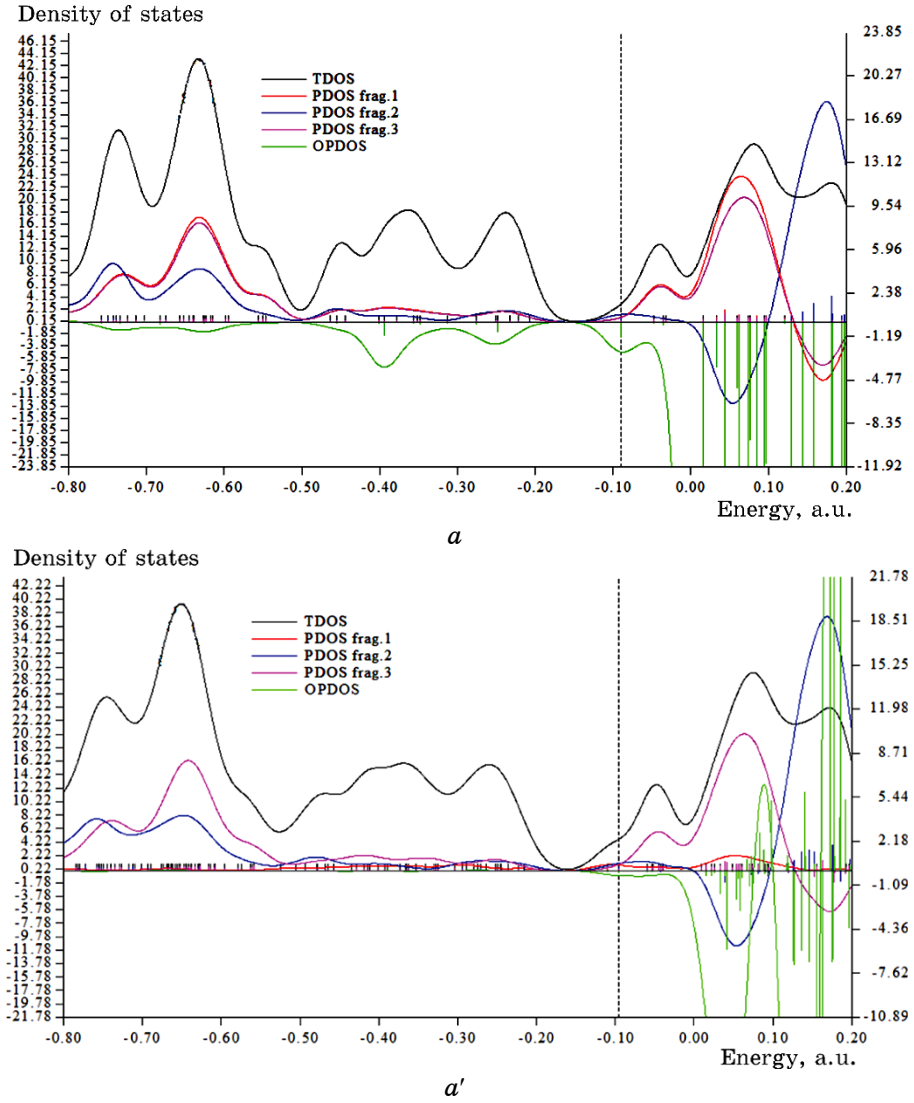

Fig. 4. TDOS/PDOS/OPDOS graphs of heteroclusters of (*a*) ZnO, (*a*′) ZnO–H_2O, (*b*) ZnS, and (*b*′) ZnS–H_2O.

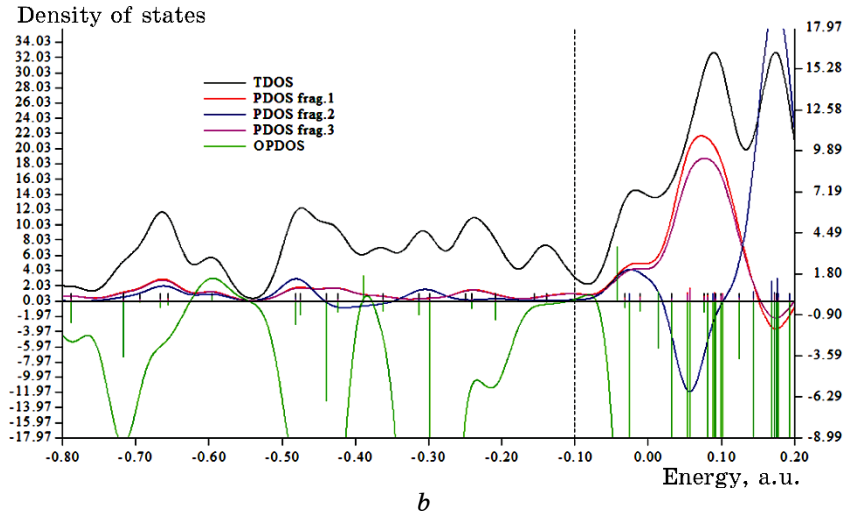

b

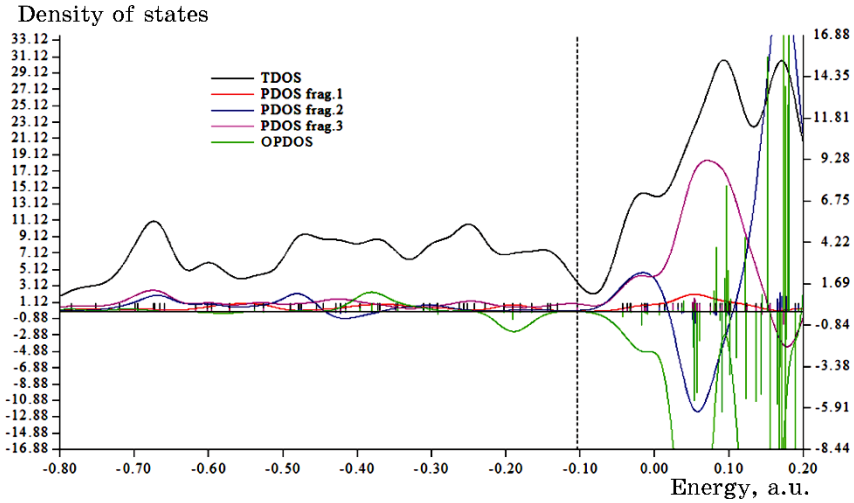

b′

Continuation Fig. 4.

part, the region around 0.1 to 0.2 a.u. has obviously larger state density than other regions for ZnS and ZnS–H_2O nanoclusters (Fig. 4, *b*, *b′*).

Fragment 1 has been defined for Zn1 (Fig. 4, *a*), O1 (Fig. 4, *a′*) and Zn2, Zn4, Zn6, Zn8, Zn10, O16, O19, O22, O24 (Fig. 4, *a*, *a′*) and H30 (Fig. 4, *a′*). Moreover, Fragment 2 has indicated the fluctuation of Zn11, Zn12, Zn13, Zn14, O17, O25, O26, O27 for ZnO and ZnO–H_2O heteroclusters (Fig. 4, *a*, *a′*) and H29 for ZnO–H_2O (Fig. 4, *a′*). Finally, it was considered the fluctuation of O15 (Fig. 4, *a*), Zn15 (Fig. 4, *a′*) and Zn3, Zn5, Zn7, Zn9, O18, O20, O21, O23

for both ZnO and ZnO–H_2O nanoclusters (Fig. 4, *a*, *a*′) through Fragment 3. Moreover, Fragment 1 has been defined for Zn1 (Fig. 4, *b*), O1 (Fig. 4, *b*′) and Zn2, Zn4, Zn6, Zn8, Zn10, S16, S19, S22, S24 (Fig. 4, *b*, *b*′) and H30 (Fig. 4, *b*′). Moreover, Fragment 2 has indicated the fluctuation of Zn11, Zn12, Zn13, Zn14, S17, S25, S26, S27 for ZnS and ZnS–H_2O heteroclusters (Fig. 4, *b*, *b*′) and H29 for ZnS–H_2O (Fig. 4, *b*′). Finally, it was considered the fluctuation of S15 (Fig. 4, *b*), Zn15 (Fig. 4, *b*′) and Zn3, Zn5, Zn7, Zn9, S18, S20, S21, S23 for both ZnS and ZnS–H_2O heteroclusters (Fig. 4, *b*, *b*′) through Fragment 3.

Localized orbital locator (LOL) has similar expression compared to electron localization function (ELF) [48]:

$$\mathrm{LOL}(\mathbf{r}) = \frac{\tau(\mathbf{r})}{1+\tau(\mathbf{r})}, \quad \tau(\mathbf{r}) = \frac{D_0(\mathbf{r})}{\frac{1}{2}\sum_i \eta_i \left|\nabla\varphi_i(\mathbf{r})\right|^2}, \tag{5}$$

$$D_0(\mathbf{r}) = \frac{3}{10}\left(6\pi^2\right)^{2/3}\left[\left(\rho_\alpha(\mathbf{r})\right)^{5/3} + \left(\rho_\beta(\mathbf{r})\right)^{5/3}\right]. \tag{6}$$

Multiwfn [49] also supports the approximate version of LOL defined by Tsirelson and Stash [50], namely, the actual kinetic energy term in LOL is replaced by second-order gradient expansion like ELF, which may demonstrate a broad span of bonding samples. This Tsirelson's version of LOL can be activated by setting 'ELFLOL_type' to 1. For special reason, if 'ELFLOL_type' in settings.ini is changed from 0 to 2, another formalism will be used:

$$\mathrm{LOL}(\mathbf{r}) = \frac{1}{1+\left(\tau(\mathbf{r})\right)^{-2}}. \tag{7}$$

If the parameter 'ELFLOL_cut' in settings.ini is set to x, then, LOL will be zero, where LOL is less than x.

The heteroclusters of ZnO/ZnO–H_2O and ZnS/ZnS–H_2O can be defined by LOL graphs owing to exploring their delocalization/localization characterizations of electrons and chemical bonds (Fig. 5, *a*, *a*′, *b*, *b*′). Covalent zones have high LOL value, the electron depletion zones between valence shell and inner shell are indicated by the blue circles around nuclei (Fig. 5, *a*, *a*′, *b*, *b*′). The counter map of LOL for ZnO/ZnO–H_2O (Fig. 5, *a*, *a*′) and ZnS/ZnS–H_2O (Fig. 5, *b*, *b*′) has shown the localized orbital locator through H/OH adsorption. ZnO–H_2O or ZnS–H_2O heterocluster indicates a larger isosurface map of the localized orbital locator due to labelling atoms of O1, Zn15, O27 or S27, H29, H30. A narrower connected area occupied by an isosurface map means that localized orbital locator is relatively difficult. However, the large counter map

of LOL for ZnO–H_2O or ZnS–H_2O can confirm that ZnO or ZnS can be a promising semiconductor material for various applications.

Moreover, intermolecular orbital overlap integral is important in discussions of intermolecular charge transfer, which can calculate HOMO–HOMO and LUMO–LUMO overlap integrals between the H/OH and heterocluster of ZnO or ZnS. The applied wave-function level is CAM–B3LYP–D3/6–311+G(d, p) that corresponds to HOMO and LUMO, respectively (Table 2).

The amount of 'Mayer bond order' [51] is generally according to empirical bond order for the single bond is near 1.0. 'Mulliken bond order' [52] with a small accord with empirical bond order is not ap-

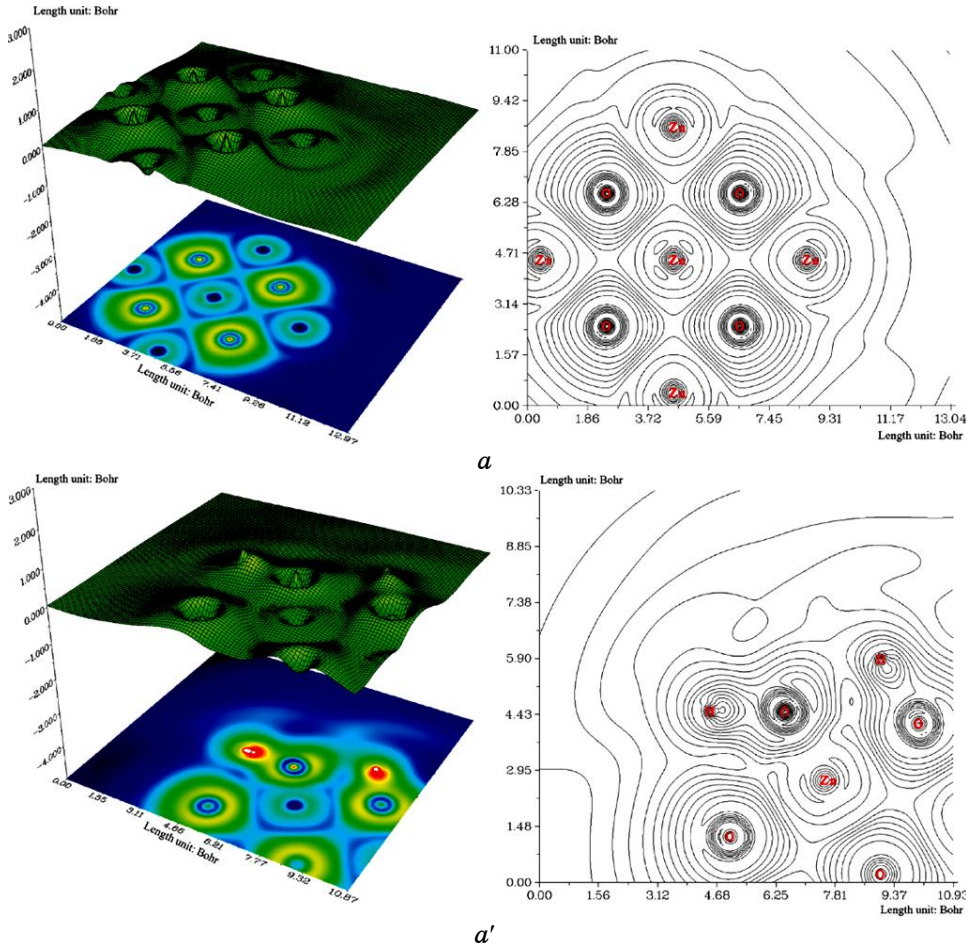

Fig. 5. The graphs of LOL for heteroclusters of (*a*) ZnO, (*a*′) ZnO–H_2O, (*b*) ZnS, and (*b*′) ZnS–H_2O. (Counter line map on the right and shaded surface map with projection in the left.)

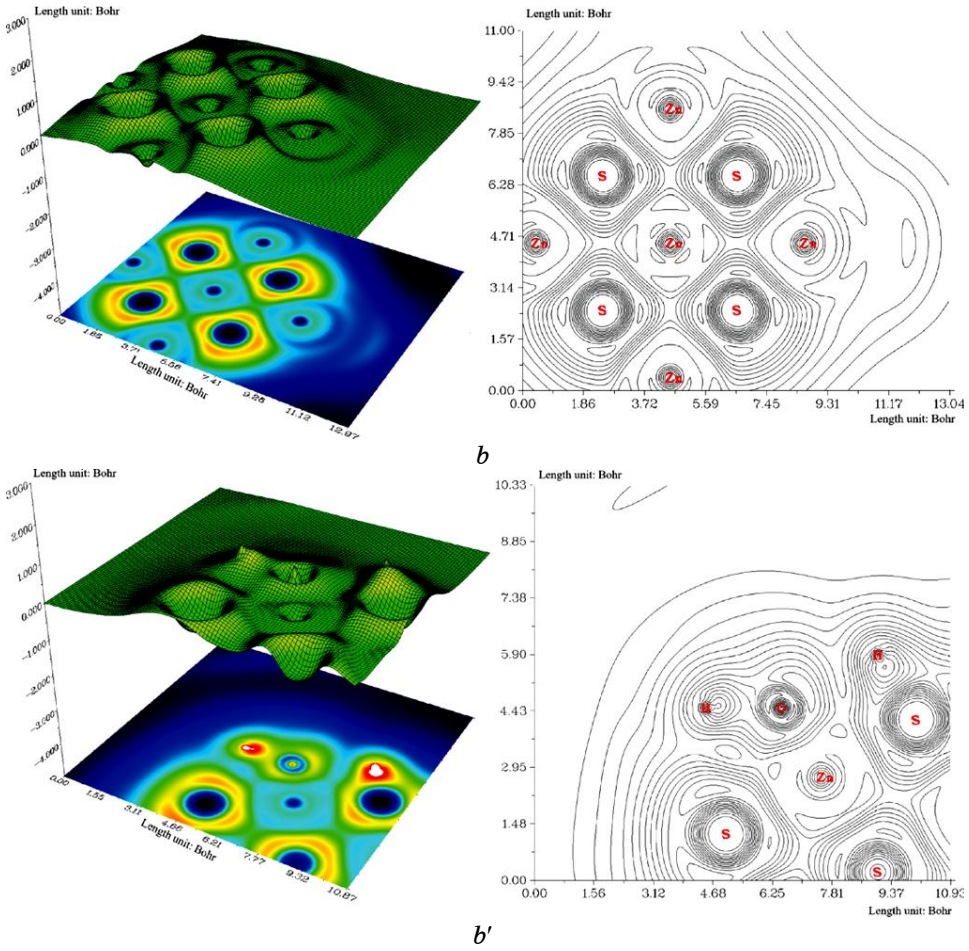

b

b′

Continuation Fig. 5.

propriate for quantifying bonding strength, for which Mayer bond order always performs better. However, 'Mulliken bond order' is a good qualitative indicator for 'positive amount' of bonding and 'negative amount' of antibonding, which are evacuated and localized, respectively (Table 3).

As it is seen in Table 3, 'Laplacian bond order' [53] has a straight cohesion with bond polarity, bond dissociation energy and bond vibrational frequency. The low value of Laplacian bond order might demonstrate that it is insensitive to the calculation degree applied for producing electron density. Generally, the value of 'Fuzzy bond order' is near Mayer bond order, especially for low-polar bonds, but much more stable with respect to the change in basis-set. Computa-

TABLE 2. LUMO, HOMO, and energy gap (ΔE) for ZnO and ZnS through H/OH adsorption and formation of ZnO–H_2O and ZnS–H_2O heteroclusters.

Heteroclusters	E_{HOMO}, eV	E_{LUMO}, eV	$\Delta E = E_{LUMO} - E_{HOMO}$, eV
ZnO	–2.4280	–1.3056	1.1223
ZnO–H_2O	–2.6110	–1.6053	1.0056
ZnS	–2.7413	–1.1723	1.5690
ZnS–H_2O	–2.7459	–1.1762	1.6696

TABLE 3. The bond orders of Mayer, Wiberg, Mulliken, Laplacian, and Fuzzy types from mixed alpha and beta density matrix for ZnO and ZnS through H/OH adsorption and formation of ZnO–H_2O and ZnS–H_2O heteroclusters.

Bond order	ZnO–H_2O			ZnS–H_2O		
	O1–Zn15	O1–H29	O27–H30	O1–Zn15	O1–H29	S27–H30
Mayer	1.1308	0.6507	0.4783	1.2782	0.6905	0.8056
Wiberg	1.7176	0.6631	0.4490	1.0554	0.6397	0.6436
Mulliken	1.9120	0.1727	0.0573	1.8753	0.1573	0.1864
Laplacian	1.6451	0.2169	0.1505	1.7453	0.2014	0.2491
Fuzzy	1.6561	0.6878	0.4321	1.5246	0.6273	0.6852

tion of 'Fuzzy bond order' demands running 'Becke's DFT' numerical integration, owing to which the calculation value is larger than assessment of 'Mayer bond order' and it can concede more precisely [54].

4. CONCLUSIONS

Considerable attention has recently been given to ZnO or ZnS as a promising multifunctional material with wide-ranging technological applications. Understanding the interaction of water with ZnO or ZnS is important for this material to be used in gas sensing, catalysis and biomedical applications. In summary, H_2O grabbing on the ZnO or ZnS was investigated by first-principles calculations. We have provided ZnO or ZnS heterocluster, and then, the geometrical parameters of H/OH adsorption on the surface of ZnO or ZnS through the absorption status and current charge density were studied. ZnO–H_2O or ZnS–H_2O heterocluster indicates a larger isosurface map of electron delocalization due to labelling atoms of O1, Zn15, O27 or S27, H29, H30. A narrower connected area occupied by an isosurface map means that electron delocalization is relatively difficult. However, the large counter map of LOL for ZnO–H_2O or

$ZnS–H_2O$ can confirm that ZnO or ZnS can be a promising semiconductor material for various applications.

ACKNOWLEDGEMENTS

In successfully completing this paper and its research, the author is grateful to Kastamonu University.

REFERENCES

1. Christopher J. Frederickson, Jae-Young Koh, and Ashley I. Bush, *Nat. Rev. Neurosci.*, 6: 449 (2005); https://doi.org/10.1038/nrn1671
2. Amir Moezzi, Andrew M. McDonagh, and Michael B. Cortie, *Chem. Eng. J.*, **185–186**: 1–22 (2012); https://doi.org/10.1016/j.cej.2012.01.076
3. Jingbin Han, Fengru Fan, Chen Xu, Shisheng Lin, Min Wei, Xue Duan, and Zhong Lin Wang, *Nanotechnology*, **21**, No. 40: 405203 (2010); https://doi.org/10.1088/0957-4484/21/40/405203
4. Zenan Jiang, Saeid Soltanian, Bobak Gholamkhass, Abdullah Aljaafari, and Peyman Servati, *RSC Adv.*, **8**, Iss. 64: 36542 (2018); https://doi.org/10.1039/C8RA07071G
5. J. Čížek, J. Valenta, P. Hruška, O. Melikhova, I. Procházka, M. Novotný, and J. Bulíř, *Appl. Phys. Lett.*, **106**: 251902 (2015); https://doi.org/10.1063/1.4922944
6. Kiyoshi Matsuyama, Kenji Mishima, Takafumi Kato, Keiichi Irie, and Kenichi Mishima, *J. Colloid Interface Sci.*, **367**: 171 (2012); https://doi.org/10.1016/j.jcis.2011.10.003
7. Buguo Wang, Bruce Claflin, Michael Callahan, Z. -Q. Fang, and David Look, *Proc. SPIE*, **8987**: 89871D (2014); https://doi.org/10.1117/12.2042344
8. B. J. Jin, S. Im, and S. Y. Lee, *Thin Solid Films*, **366**: 107 (2000); https://doi.org/10.1016/S0040-6090(00)00746-X
9. C. V. Manzano, D. Alegre, O. Caballero-Calero, B. Alén, and M. S. Martín-González, *J. Appl. Phys.*, **110**: 043538 (2011); https://doi.org/10.1063/1.3622627
10. M. A. Borysiewicz, M. Wzorek, T. Wojciechowski, T. Wojtowicz, E. Kamińska, and A. Piotrowska, *J. Lumin.*, **147**: 367 (2014); https://doi.org/10.1016/j.jlumin.2013.11.076
11. Oscar Marin, Vanessa González, Mónica Tirado, and David Comedi, *Mater. Lett.*, **251**: 41 (2019); https://doi.org/10.1016/j.matlet.2019.05.033
12. Huan-Ming Xiong, Da-Peng Liu, Yong-Yao Xia, and Jie-Sheng Chen, *Chem. Mater.*, **17**: 3062 (2005); https://doi.org/10.1021/cm050556r
13. D. C. Agarwal, U. B. Singh, Srashti Gupta, Rahul Singhal, P. K. Kulriya, Fouran Singh, A. Tripathi, Jitendra Singh, U. S. Joshi, and D. K. Avasthi, *Scientific Reports*, **9**: 6675 (2019); https://doi.org/10.1038/s41598-019-43184-9
14. E. Wolska, J. Kaszewski, P. Kiełbik, J. Grzyb, M. M. Godlewski, and M. Godlewski, *Opt. Mater.*, **36**: 1655 (2014); https://doi.org/10.1016/j.optmat.2013.12.032

15. J.-H. Lim, C.-K. Kang, K.-K. Kim, I.-K. Park, D.-K. Hwang, and S.-J. Park, *Adv. Mater.*, **18**: 2720 (2006); https://doi.org/10.1002/adma.200502633
16. Diana B. Tolubayeva, Lesya V. Gritsenko, Yevgeniya Y. Kedruk, Madi B. Aitzhanov, Renata R. Nemkayeva, and Khabibulla A. Abdullin, *Biosensors*, **13**: 793 (2023); https://doi.org/10.3390/bios13080793
17. Haijie Liu, Yan Zhang, Haihua Zhang, Longcai Wang, Tao Wang, Zhifa Han, Liyong Wu, and Guiyou Liu, *J. Transl. Med.*, **19**: 221 (2021); https://doi.org/10.1186/s12967-021-02892-5
18. Kh. A. Abdullin, M. T. Gabdullin, L. V. Gritsenko, D. V. Ismailov, Zh. K. Kalkozova, S. E. Kumekov, Zh. O. Mukash, A. Yu. Sazonov, and E. I. Terukov, *Semiconductors*, **50**: 1010 (2016); https://doi.org/10.1134/S1063782616080029
19. Shang-Chou Chang, Jhih-Ciang Hu, Huang-Tian Chan, and Chuan-An Hsiao, *Coatings*, **12**: 945 (2022); https://doi.org/10.3390/coatings12070945
20. Shang-Chou Chang, Tsung-Han Li, and Huang-Tian Chan, *Int. J. Electrochem. Sci.*, **16**: 210817 (2021); https://doi.org/10.20964/2021.08.34
21. Cong Zhang, Zongsheng Cao, Guangliang Zhang, Yu Yan, Xin Yang, Jiayuan Chang, Yanfei Song, Yuhang Jia, Peng Pan, Wei Mi, Zhengchun Yang, Jinshi Zhao, and Jun Wei, *Microchem. J.*, **158**: 105237 (2020); https://doi.org/10.1016/j.microc.2020.105237
22. Srijita Nundy, Aritra Ghosh, and Tapas K. Mallick, *ACS Omega*, **5**, No. 2: 1033 (2020); https://doi.org/10.1021/acsomega.9b02758
23. David Raymand, Adri C. T. van Duin, Daniel Spångberg, William A. Goddard III, and Kersti Hermansson, *Surface Science*, **604**, Nos. 9–10: 741 (2010). https://doi.org/10.1016/j.susc.2009.12.012
24. Gang Wang, Baibiao Huang, Zhujie Li, Zaizhu Lou, Zeyan Wang, Ying Dai, and Myung-Hwan Whangbo, *Scientific Reports*, **5**: 8544 (2015); doi:10.1038/srep08544
25. Afaq Ullah Khan, Kamran Tahir, Karma Albalawi, Mona Y. Khalil, Zainab M. Almarhoon, Magdi E. A. Zaki, Salman Latif, Hassan M. A. Hassan, Moamen S. Refat, and Alaa M. Munshi, *Materials Chemistry and Physics*, **291**: 126667 (2022); https://doi.org/10.1016/j.matchemphys.2022.126667
26. Dejan Zagorac, Jelena Zagorac, Milan Pejić, Branko Matović, and Johann Christian Schön, *Nanomaterials*, **12**: 1595 (2022); https://doi.org/10.3390/nano12091595
27. Nicolas Perciani de Moraes, Lucca Gabriel Penida Marins, Marcelo Yuji de Moura Yamanaka, Rebeca Bacani, Robson da Silva Rocha, and Liana Alvares Rodrigues, *J. Photochem. Photobiol. A Chem.*, **418**: 113377 (2021); https://doi.org/10.1016/j.jphotochem.2021.113377
28. Asset Bolatov, Alida Manjovelo, Bilel Chouchene, Lavinia Balan, Thomas Gries, Ghouti Medjahdi, Bolat Uralbekov, and Raphaël Schneider, *Materials*, **17**: 4877 (2024); https://doi.org/10.3390/ma17194877
29. Zhifang Dong, Yan Wu, Natarajan Thirugnanam, and Gonglin Li, *Appl. Surf. Sci.*, **430**: 293 (2018); https://doi.org/10.1016/j.apsusc.2017.07.186
30. P. E. Blöchl, *Phys. Rev. B*, **50**: 17953 (1994); https://doi.org/10.1103/PhysRevB.50.17953
31. J. P. Perdew, K. Burke, and M. Ernzerhof, *Phys. Rev. Lett.*, **77**: 3865 (1996); https://doi.org/10.1103/PhysRevLett.77.3865
32. Paul Ziesche, Stefan Kurth, and John P. Perdew, *Comput. Mater. Sci.*, **11**:

122 (1998); https://doi.org/10.1016/S0927-0256(97)00206-1
33. Marco Arrigoni and Georg K. H. Madsen, *Comput. Mater. Sci.*, 156: 354 (2019); https://doi.org/10.1016/j.commatsci.2018.10.005
34. P. Hohenberg and W. Kohn, *Phys. Rev. B*, 136: B864 (1964); https://doi.org/10.1103/PhysRev.136.B864
35. W. Kohn and L. J. Sham, *Phys. Rev.*, **140**: A1133 (1965); https://doi.org/10.1103/PhysRev.140.A1133
36. Axel D. Becke, *J. Chem. Phys.*, **98**: 5648 (1993); https://doi.org/10.1063/1.464913
37. Chengteh Lee, Weitao Yang, and Robert G. Parr, *Phys Rev B*, **37**: 785 (1988); https://doi.org/10.1103/PhysRevB.37.785
38. K. Kim and K. D. Jordan, *J. Phys. Chem.*, **98**, No. 40: 10089 (1994); https://doi.org/10.1021/j100091a024
39. P. J. Stephens, F. J. Devlin, C. F. Chabalowski, and M. J. Frisch, *J. Phys. Chem.*, **98**, No. 45: 11623 (1994); https://doi.org/10.1021/j100096a001
40. C. J. Cramer, *Essentials of Computational Chemistry: Theories and Models* (Wiley: 2004).
41. Fatemeh Mollaamin and Majid Monajjemi, *Int. J. Quantum Chem.*, **124**: e27348 (2024); https://doi.org/10.1002/qua.27348
42. Fatemeh Mollaamin and Majid Monajjemi, *Molecular Simulation*, **49**, 4: 365 (2023); https://doi.org/10.1080/08927022.2022.2159996
43. S. H. Vosko, L. Wilk, and M. Nusair, *Can. J. Phys.*, **58**, No. 8: 1200 (1980); https://doi.org/10.1139/p80-159
44. M. J. Frisch, G. W. Trucks, H. B. Schlegel, G. E. Scuseria, M. A. Robb et al., *Gaussian 16, Revision C.01* (Wallingford CT: Gaussian, Inc.: 2016).
45. R. Dennington, T. A. Keith, and J. M. Millam, *GaussView 6.0.16* (Semichem Inc.: 2016).
46. Zihan Xu, Chenglong Qin, Yushu Yu, Gang Jiang, and Liang Zhao, *AIP Advances*, **14**: 055114 (2024); https://doi.org/10.1063/5.0208082
47. A. D. Becke and K. E. Edgecombe, *J. Chem. Phys.*, 9: 5397 (1990); https://doi.org/10.1063/1.458517
48. H. L. Schmider and A. D. Becke, *Journal of Molecular Structure: THEOCHEM.*, **527**, Nos. 1–3: 51 (2000); https://doi.org/10.1016/S0166-1280(00)00477-2
49. A. D. Becke and K. E. Edgecombe, *J. Chem. Phys.*, **9**: 5397 (1990); https://doi.org/10.1063/1.458517
50. V. Tsirelson and A. Stash, *Acta Cryst.*, **B58**: 780 (2002); https://doi.org/10.1107/S0108768102012338
51. I. Mayer, *Chemical Physics Letters*, **544**: 83 (2012); https://doi.org/10.1016/j.cplett.2012.07.003
52. F. Mollaamin, M. T. Baei, M. Monajjemi, R. Zhiani, and B. Honarparvar, *Russ. J. Phys. Chem.*, **82**, 2354 (2008); https://doi.org/10.1134/S0036024408130323
53. Tian Lu and Feiwu Chen, *J. Phys. Chem. A*, **117**: No. 14: 3100 (2013); https://doi.org/10.1021/jp4010345
54. Xiyi Wang, Xuefeng Zhang, Witold Pedrycz, Shuang-Hua Yang, and Driss Boutat, *Fractal Fract.*, **8**: 523 (2024); https://doi.org/10.3390/fractalfract8090523